Nanoscale

PAPER

View Article Online
View Journal | View Issue

Cite this: *Nanoscale*, 2015, **7**, 15953

Aptamer loaded MoS_2 nanoplates as nanoprobes for detection of intracellular ATP and controllable photodynamic therapy†

Li Jia,‡ Lin Ding,‡ Jiangwei Tian, Lei Bao, Yaoping Hu, Huangxian Ju* and Jun-Sheng Yu*

Received 7th April 2015,
Accepted 15th May 2015

DOI: 10.1039/c5nr02224j

www.rsc.org/nanoscale

In this work we designed a MoS_2 nanoplate-based nanoprobe for fluorescence imaging of intracellular ATP and photodynamic therapy (PDT) *via* ATP-mediated controllable release of $^1O_2$. The nanoprobe was prepared by simply assembling a chlorine e6 (Ce6) labelled ATP aptamer on MoS_2 nanoplates, which have favorable biocompatibility, unusual surface-area-to-mass ratio, strong affinity to single-stranded DNA, and can quench the fluorescence of Ce6. After the nanoprobe was internalized into the cells and entered ATP-abundant lysosomes, its recognition to ATP led to the release of the single-stranded aptamer from MoS_2 nanoplates and thus recovered the fluorescence of Ce6 at an excitation wavelength of 633 nm, which produced a highly sensitive and selective method for imaging of intracellular ATP. Meanwhile, the ATP-mediated release led to the generation of $^1O_2$ under 660 nm laser irradiation, which could induce tumor cell death with a lysosomal pathway. The controllable PDT provided a model approach for design of multifunctional theranostic nanoprobes. These results also promoted the development and application of MoS_2 nanoplate-based platforms in biomedicine.

Introduction

In recent years, transition metal dichalcogenides (TMDCs)[1–3] have received tremendous attention due to their fantastic physical properties, which result from a quantum size effect connected with their ultra-thin structure.[4] TMDCs, such as MoS_2, $MoSe_2$, WS_2, and WSe_2, TiS_2, TaS_2, and ZrS_2, all are made up of a hexagonal plane of positively charged transition metal atoms M sandwiched between two planes of negatively charged chalcogen atoms (X) with the stoichiometry MX_2.[1,5] Owing to the strong covalent bonding within each layer and the weak van der Waals forces between layered structures,[6] these materials exhibit versatile and unique properties including carrier mobility, electronic, optical, catalytic, mechanical and chemical properties.[6–9] This promises their potential applications in many different fields, ranging from energy storage,[10–12] electronics,[10,13–15] catalysis,[16–19] sensing[10,20,21] to biomedicine.[5,20,22]

In biomedical area, TMDCs have become rising stars due to their outstanding properties, analogous to graphene. For example, single-layered MoS_2 nanosheets with excellent fluorescence quenching ability have been employed for the detection of biomolecules.[20] As strong near-infrared (NIR) light-absorbing agents, MoS_2,[23–25] Bi_2Se_3,[26] and WS_2 [5] nanosheets have been used to kill cancer cells *in vitro* and *in vivo* by functionalization with different groups. More recently, a multifunctional MoS_2-IO-(d)PEG nanocomposite, iron oxide decorated with MoS_2 nanosheets with dual PEG coatings, achieved efficient triple modal imaging-guided photothermal therapy.[27] Moreover, the unusual surface-area-to-mass ratio of TMDCs makes them highly suitable for delivering drug molecules, for instance chemotherapy drug doxorubicin (DOX),[23,28] photodynamic agent chlorine e6 (Ce6), *etc*.[25,28] Compared with popularly used carbon nanomaterials such as graphene oxide, MoS_2 nanoplates are much less hazardous,[29] underlining the great advantage of their application in biomedicine. Moreover, smaller MoS_2 nanoplates can be more easily and rapidly internalized into cells than big ones.[30] Their high quenching ability toward fluorescence[20] *via* energy transfer can be used to design different nanoprobes for the detection of biomolecules. This work used a chlorine e6 (Ce6) labelled ATP aptamer to functionalize MoS_2 nanoplates and developed a nanoprobe for fluorescence imaging of intracellular ATP. More interestingly, the release of a Ce6 labelled ATP aptamer from MoS_2 nano-

State Key Laboratory of Analytical Chemistry for Life Science, School of Chemistry and Chemical Engineering, Nanjing University, Nanjing 210093, P. R. China. E-mail: hxju@nju.edu.cn, jsyu@nju.edu.cn; Fax: +86 (25) 83593593; Tel: +86 (25) 83593593

†Electronic supplementary information (ESI) available: Supplementary figures. See DOI: 10.1039/c5nr02224j

‡These authors contributed equally to this work.

plates upon the recognition of the nanoprobe to ATP led to the generation of $^1O_2$ under 660 nm laser irradiation (Scheme 1). Thus a novel method for cancer photodynamic therapy was proposed.

ATP is an essential biogenic biomolecule and plays important roles in a variety of biological processes.[31,32] The concentration of intracellular ATP ranging from 1 to 10 mM is much greater than that in body fluids (<5 μM).[33] The distinct difference of the ATP levels provides a significant principle for designing ATP-mediated drug delivery platforms.[33,34] Ce6, as a typical second-generation photosensitizer, has good optical properties, high photosensitizing efficacy, and low dark toxicity.[35] Upon irradiation with appropriate light, Ce6 can be activated to produce $^1O_2$, the cytotoxic reactive oxygen species (ROS). Furthermore, it can emit strong fluorescence at a wavelength range of 660 to 670 nm, where hemoglobin and water absorb weakly.[30] By the use of the superior characteristics of MoS_2 nanoplates and Ce6, the strong adsorption of single-stranded aptamers on MoS_2 nanoplates, and the importance of ATP, the smart nanoprobe was endowed with ATP-responsive fluorescence switch and ATP-mediated controllable release of $^1O_2$. After the nanoprobe was taken up by cancer cells and accumulated in ATP-abundant lysosomes,[36] the recognition of the nanoprobe to ATP led to the release of the Ce6-aptamer to recover Ce6 fluorescence and activate Ce6 for producing $^1O_2$. This work provides a promising approach to design multifunctional theranostic nanoprobes for imaging of intracellular biomolecules and photodynamic therapy.

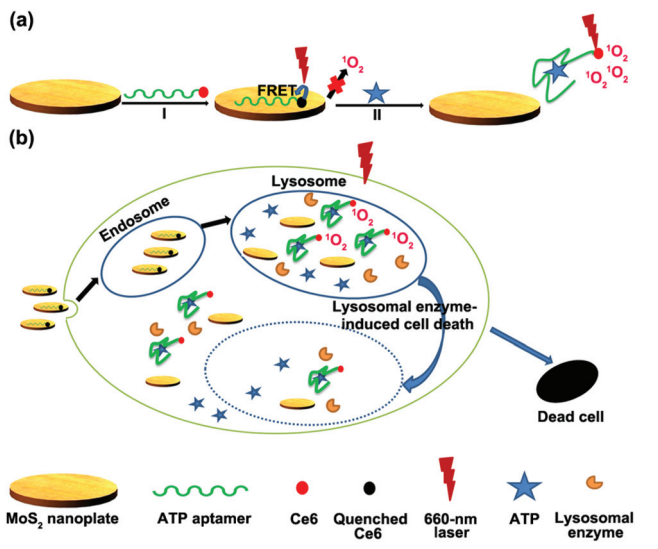

Scheme 1 (a) Schematic illustration of the Ce6-aptamer loaded MoS_2 nanoprobe for $^1O_2$ production upon target binding. (b) Endocytosis of the nanoprobe for ATP imaging and ATP-mediated release of $^1O_2$ in lysosomes under 660 nm laser irradiation, which leads to the lysosomal enzyme-induced cell death. The $^1O_2$ induces the lysosomal membrane permeabilization and consequent release of lysosomal enzymes into the cytosol to trigger apoptosis.

Experimental

Materials and reagents

The Ce6-aptamer (5′-Ce6-AAC CTG GGG GAG TAT TGC GGA GGA AGG T-3′) and the Ce6-labeled random DNA (Ce6-R, 5′-Ce6-AAA AAA GCT TGT GTT CGT TGG AAA AAA A-3′) were synthesized by TaKaRa Biotechnology Co., Ltd (Dalian, China). ATP, uridine triphosphate (UTP), cytidine triphosphate (CTP), guanosine triphosphate (GTP), methylene blue (MB), Hoechst 33342, MoS_2 powder (99%, 2 μm in size), propidium iodide (PI), 4-(2-hydroxyethyl)-1-piperazineethanesulfonic acid (HEPES), dimethylformamide (DMF), dimethyl sulfoxide (DMSO) and vitamin C were purchased from Sigma Aldrich. 1,3-Diphenylisobenzofuran (DPBF) was purchased from Alfa Aesar (Ward Hill, MA, USA). LysoTracker Green DND-26 and singlet oxygen sensor green (SOSG) were obtained from Invitrogen (Carlsbad, CA, USA). 3-(4,5-Dimethylthiazol-2-yl)-2,5-diphenyltetrazolium bromide (MTT) and Annexin V-FITC/PI cell apoptosis kit were purchased from KeyGen Biotech. Co. Ltd (Nanjing, China). Oligomycin was purchased from Sangon Biological Engineering Technology & Co. Ltd (Shanghai, China). The HEPES buffer (pH 7.4) contained 10 mM HEPES, 137 mM NaCl, 2.7 mM KCl and 5 mM $MgCl_2$ unless otherwise noted. All other reagents were of analytical grade and used without further purification. All solutions were prepared using ultrapure water, which was obtained using a Millipore Simplicity System (Millipore, Bedford, USA). The concentrations were all final concentrations unless otherwise noted.

Apparatus

The morphology of the MoS_2 nanoplates was characterized using a JEM-2100 transmission electron microscope (JEOL Ltd, Japan). Dynamic light scattering (DLS) measurement was performed on 90 Plus/BI-MAS equipment (Brookhaven, USA). Zeta potential analysis was performed at room temperature on a Zetasizer (Nano-Z, Malvern, UK). UV-vis-NIR spectra were measured on a UV-3600 spectrophotometer (Shimadzu, Japan). Atomic force microscopic (AFM) measurements were performed in ScanAsyst mode on Fastscan AFM (Bruker, Inc.) by directly casting the sample dispersion onto the mica sheet. The fluorescence spectra were obtained on a RF-5301PC spectrofluorometer (Shimadzu, Japan) equipped with a xenon lamp. Flow cytometric analysis was performed on a Coulter FC-500 flow cytometer (Beckman-Coulter). Gel electrophoresis was performed on a DYCP-31 BN electrophoresis analyser (Liuyi Instrument Company, China) and imaged on the Bio-Rad ChemDoc XRS (USA). The cell images were observed using a Leica TCS SP5 confocal laser scanning microscope (CLSM, Germany). The MTT assay was performed using a Varioskan Flash microplate reader (ThermoFisher Scientific) at 490 nm.

Preparation and fluorescence quenching ability of MoS_2 nanoplates

Small MoS_2 nanoplates were prepared by a modified liquid exfoliation method.[2] 300 mg MoS_2 powder was mixed with 100 mL of ethanol/water with an ethanol volume fraction of

45% in a 250 ml flask. The mixture in the sealed flask was ultrasonicated for 24 h to form a dark green suspension. After that, the dispersion was centrifuged at 6000 rpm for 20 min three times to remove the aggregates. Then the supernatant was collected and baked at 70 °C in an oven to get rid of the ethanol and water successively. Next, the product was dissolved in water and then centrifuged at 6000 rpm twice to remove the larger MoS_2 nanoparticles. Lastly, the supernatant was filtered through a 0.22 μm Millipore membrane filter. The prepared MoS_2 nanoplates were stored at 4 °C. Their fluorescence quenching ability was examined by mixing MoS_2 nanoplates ranging from 0 to 70 μg mL^{-1} with 200 nM Ce6-aptamer in HEPES buffer (20 mM, pH 7.4) to measure the fluorescence spectra from 620 to 720 nm with excitation at 404 nm.

Preparation of aptamer loaded MoS_2 nanoplates

MoS_2 nanoplates of 400 μg mL^{-1} were incubated with 2.0 μM Ce6-aptamer overnight, and then the conjugate was centrifuged at 12 000 rpm for 30 min and washed with ultrapure water five times to remove the free Ce6-aptamer. The obtained nanoprobe (1.52 μM Ce6 equiv.) was stored at 4 °C. The loading amount of the Ce6-aptamer on MoS_2 nanoplates was obtained by measuring the amount of the Ce6-aptamer left in the waste solution at 404 nm, where Ce6 has a strong molar extinction coefficient of 1.10×10^5 M^{-1} cm^{-1}. A control MoS_2/Ce6-R nanocomplex was also prepared by the same procedure using a Ce6-labeled random DNA (Ce6-R) to replace the Ce6-aptamer.

Fluorescence response and selectivity of the nanoprobe toward ATP

After the nanoprobe (200 nM Ce6 equiv.) was incubated with different concentrations of ATP ranging from 0 to 3 mM in HEPES buffer (20 mM, pH 7.4) at room temperature for 2 h, the fluorescence measurement was carried out from 600 to 750 nm with the excitation wavelength at 404 nm at room temperature. To evaluate the selectivity, each type of nucleotide (ATP, CTP, UTP, GTP) of 1 mM was incubated with the nanoprobe (200 nM Ce6 equiv.) for 2 h to measure the fluorescence intensity at 663 nm, respectively.

Singlet oxygen generation and quantum yield

Singlet oxygen quantum yield was determined by monitoring the photooxidation of DPBF. The experiment was performed as follows: MB (3.0 μM), Ce6-aptamer (3.0 μM Ce6 equiv.), MoS_2 (800 μg mL^{-1}), nanoprobe (3.0 μM Ce6 equiv.), and nanoprobe (3.0 μM Ce6 equiv.) with 2 mM ATP in the HEPES buffer (20 mM, pH 7.4) were respectively mixed with 30 μM DPBF and subsequently oxygen-saturated in the dark. Following this, the solutions were irradiated with a 660 nm laser at a light power density of 0.5 W cm^{-2} in the time interval of 30 s. The singlet oxygen quantum yields were measured using MB in DMF (Φ = 0.52) as the standard and calculated using eqn (1):[37]

$$\Phi_X = \Phi_{MB}\left(\frac{S_X}{S_{MB}}\right)\left(\frac{F_{MB}}{F_X}\right) \quad (1)$$

where the subscript X denotes the test, Φ stands for the singlet oxygen quantum yield, S stands for the slope of the different absorbance changes of DPBF (at 410 nm) with the irradiation time, and F stands for the absorption correction factor, which is based on $F = 1–10^{-OD}$ (OD is the absorbance of the test or MB at 660 nm).

Cell culture

Human cervical carcinoma HeLa cell line was purchased from KeyGen Biotech Co., Ltd (Nanjing, China) and cultured in a flask in Dulbecco's modified Eagle's medium (DMEM) containing 10% fetal bovine serum (FBS), 100 μg mL^{-1} streptomycin, 100 U mL^{-1} penicillin at 37 °C under a humidified atmosphere containing 5% CO_2. The medium was refreshed every two days and the cells were subcultured after reaching confluence.

MTT assays

The MTT assay was carried out to investigate the biocompatibility of MoS_2 nanoplates and graphene oxide (GO), and the dark toxicity and phototoxicity of the nanoprobe. HeLa cells were seeded in four 96-well culture plates at 1×10^4 per well for 24 h. After rinsing with HEPES buffer, the solutions of MoS_2, GO, and the nanoprobe at a series of concentrations were respectively added to each of the plates. For measurement of the biocompatibility of MoS_2 nanoplates and GO, the two nanomaterials were incubated with the cells for 24 h separately. For the dark toxicity and phototoxicity study of the nanoprobe, after incubation with the cells for 6 h, one plate containing the nanoprobe was irradiated using a 660 nm laser at a power density of 0.22 W cm^{-2} for 5 min, and the other plate was kept in the dark. The two plates were then subjected to 24 h incubation. For MTT measurements, 40 μL of 5 mg mL^{-1} MTT solution in pH 7.4 PBS was added to each well of each plate. Four hours later, the medium was removed and replaced with 200 μL DMSO to dissolve blue formazan. After 1 h the optical density (OD) at 490 nm was measured. The cell viability was then assessed by eqn (2):

$$\text{cell viability}(\%) = \frac{\text{OD value of treatment group}}{\text{OD value of control group}} \times 100\% \quad (2)$$

The percentage of growth inhibition was determined using eqn (3):

$$\text{growth inhibition}(\%) = \left(1 - \frac{\text{OD value of treatment group}}{\text{OD value of control group}}\right) \times 100\% \quad (3)$$

Phototoxicity assay

HeLa cells were seeded on 6-well plates at 1×10^5 cells per well and cultured in complete medium for 24 h at 37 °C. Next, the medium was removed and replaced with the nanoprobe (2.0 μM Ce6 equiv.) in HEPES buffer. After incubation for 6 h at 37 °C, the cells were subjected to irradiation under a

660 nm laser at a power of 0.22 W cm^{-2} for 100, 200, and 300 s respectively. Then, the cells were stained with Annexin V-FITC/PI on the basis of the instruction, trypsinized, collected, washed with PBS, resuspended, and examined by flow cytometric assays. All experiments were performed with at least 10 000 cells.

Cell imaging

For cell imaging experiments, the HeLa cells were seeded into 35 mm confocal dishes (Glass Bottom Dish) at 1×10^4 cells per dish and grown for 24 h at 37 °C. Then the cells were washed three times with HEPES buffer. Prior to the addition of the nanoprobe, the cells were incubated with or without 10 μg mL^{-1} oligomycin or 5 mM Ca^{2+} for 30 min. Afterward, the medium was replaced with 200 μL of nanoprobe (2.0 μM Ce6 equiv.), and MoS_2/Ce6-R nanocomplex (2.0 μM Ce6 equiv.) (a control nanoprobe) or Ce6-aptamer (2.0 μM Ce6 equiv.), respectively. Six hours later, the cells were rinsed three times with the HEPES buffer and imaged on a CLSM with the emission collected from 640 to 700 nm under excitation at 633 nm.

Subcellular localization of the nanoprobe

After incubating HeLa cells with the nanoprobe for 6 h, the subcellular localization of the nanoprobe was performed by staining the nanoprobe-loaded cells with 2 μM LysoTracker Green DND-26 and 2 μM Hoechst 33342 for 20 min simultaneously. After washing five times, the cells were observed by CLSM. Hoechst 33342 was excited by using a 405 nm laser and collected within the range of 420–480 nm. LysoTracker Green DND-26 was excited by using a 488 nm argon ion laser, and the emission was collected from 505 to 535 nm.

PDT efficacy of the nanoprobe

To examine the PDT efficacy of the nanoprobe and the role of $^1O_2$ in PDT, HeLa cells in 35 mm confocal dishes were divided into 6 groups for the following treatments: group 1, untreated; group 2, treated with 66 J cm^{-2} irradiation with a 660 nm laser; group 3, cultured with the nanoprobe (2.0 μM Ce6 equiv.) without laser irradiation; group 4, cultured with the nanoprobe (2.0 μM Ce6 equiv.) and combined with 66 J cm^{-2} irradiation successively; group 5, treated with 10 μg mL^{-1} oligomycin first, and then incubated with the nanoprobe (2.0 μM Ce6 equiv.) in combination with 66 J cm^{-2} irradiation; group 6, cultured with the nanoprobe (2.0 μM Ce6 equiv.) and then vitamin C plus the 66 J cm^{-2} irradiation. Afterwards, the cells in dishes were stained with PI, and the cell death was visualized with CLSM. Besides, the HeLa cells with different treatments were also analysed by MTT assays.

To prove that cell death was caused by the PDT rather than the photothermal effect or the synergistic therapy, the temperature change of the MoS_2 nanoplate solution (400 μg mL^{-1}) and ultrapure water was recorded every 1 min during the 8 min laser irradiation at 660 nm.

Polyacrylamide hydrogel electrophoresis

The nanoprobe (6.0 μM Ce6 equiv.) was incubated with or without 1.5 mM ATP for 2 h, and then centrifuged at 12 000 rpm for 30 min to obtain the supernatants. Gel electrophoresis was performed by adding 7 μL of Ce6-aptamer (6.0 μM Ce6 equiv.) or the two different supernatants to a mixture of 1.5 μL loading buffer and 1.5 μL GelRed, respectively. After that, the mixtures were separately injected into polyacrylamide hydrogel in tris-borate-EDTA (TBE) buffer. Electrophoresis was run for 1 h at 100 V. The fluorescence images of gels were observed by Ce6 fluorescence analysis under UV irradiation.

Statistical analysis

All the data were shown as means ± SD through at least three experiments. Statistical analysis was performed with a statistics program (GraphPad Prism; GraphPad Software). $P < 0.05$ was regarded as statistically significant.

Results and discussion

Characterization of MoS_2 nanoplates and the nanoprobe

The liquid exfoliation method is an efficient way to break the weak interlayer forces in bulk materials to obtain 2D nanosheets and small nanoparticles by simple sonication in commonly used solvents.[1,17,38,39] Herein, small MoS_2 nanoplates were synthesized by ultrasonication in a mixture of ethanol and water followed by removal of large-sized particles by centrifugation.[2] The TEM image of the resulting MoS_2 nanoplates showed a well-dispersed round-shaped morphology with an average diameter of 7.3 nm (Fig. 1a) and a lattice fringe spacing of 2.7 Å (inset in Fig. 1a), corresponding to the (100) planes of MoS_2 nanoparticles.[4,39] The mean hydrodynamic diameter of the nanoplates was 22.4 nm measured by DLS (Fig. 1b), which was larger than that of TEM results due to the presence of the solvation layer. The AFM measurements indicated that the thickness of the MoS_2 nanoplates was around 0.9 nm (Fig. 1c), suggesting the 2-D layered structure of the prepared MoS_2 nanoplates.[2,40] The zeta potential of the nanoplates was determined to be −28.5 mV (Fig. 2a), suggesting great colloidal stability in aqueous media.

The nanoprobe was prepared through the strong interaction of the Ce6-aptamer with MoS_2. Both MoS_2 nanoplates and the nanoprobe showed the absorption at 607 and 665 nm (Fig. 2b) in accordance with the characteristic peaks of exfoliated MoS_2 nanoparticles.[2] The absorption spectrum of the Ce6-aptamer exhibited a strong Ce6 characteristic absorption peak at 404 nm with a molar absorption coefficient of 1.10×10^5 M^{-1} cm^{-1} and the characteristic peak of DNA at 255 nm.[41] The AFM measurement revealed that the height of the nanoprobe was about 1.4 nm (Fig. 1d), greater than 0.9 nm of the MoS_2 nanoplates. These results verified the successful assembly of the Ce6-aptamer on the surface of MoS_2 nanoplates. Moreover, the amount of Ce6-aptamer loaded on MoS_2 nanoplates reached 3.80 nmol mg^{-1}, which is close to the loading amount of 4.00 nmol mg^{-1} reported on the graphene oxide.[42]

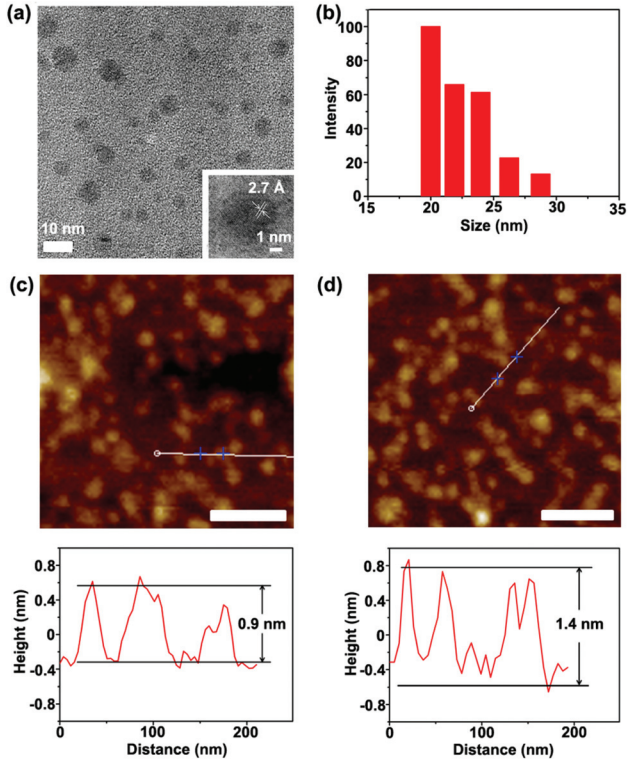

Fig. 1 (a) HRTEM image of MoS_2 nanoplates. Inset: HRTEM image highlighting the 2.7 Å lattice fringes that correspond to the (100) planes. (b) DLS characterization of the prepared MoS_2 nanoplates. AFM characterization of (c) MoS_2 and (d) nanoprobe, and the corresponding height images. Scale bar: 100 nm.

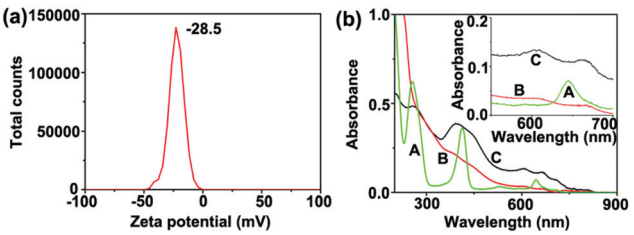

Fig. 2 (a) Zeta potential distribution of MoS_2 nanoplates. (b) UV-vis-NIR spectra of (A) Ce6-aptamer, (B) MoS_2, and (C) nanoprobe. Inset: the absorbance of A, B, and C in the wavelength range of 550 to 700 nm.

The quenching capability of the MoS_2 nanoplates on Ce6 fluorescence was also demonstrated. The Ce6 fluorescence signal gradually reduced with the increasing concentration of MoS_2 nanoplates in 200 nM Ce6-aptamer solution (Fig. S1†), indicating an increased amount of Ce6-aptamer adsorbed. When the concentration of MoS_2 reached 40 μg mL^{-1}, the fluorescence of Ce6 was largely quenched.

Fluorescence response toward ATP

To test the response of the probe to ATP, the fluorescence intensities (FI) of the mixtures of the nanoprobe and different concentrations of ATP were recorded. The FI gradually increased with the increasing concentration of ATP in the range of 5 μM to 3 mM (Fig. 3a and b). This fluorescence change could be attributed to the higher affinity of the ATP aptamer toward ATP compared with MoS_2 nanoplates. When ATP was absent, the aptamer, presenting an unfolded and flexible structure, was prone to adsorption on MoS_2. In the presence of ATP, the Ce6-aptamer bound with ATP to form a folded and rigid structure. This resulted in the release of the Ce6-aptamer from the MoS_2 and thus the fluorescence of Ce6 was recovered. The ATP-triggered aptamer release could also be verified by gel electrophoresis (Fig. S2†). After mixing ATP with the nanoprobe, the supernatant displayed an obvious band for the aptamer complex (lane c in Fig. S2†), indicating the departure of the aptamer from MoS_2 and the binding of the aptamer with ATP.

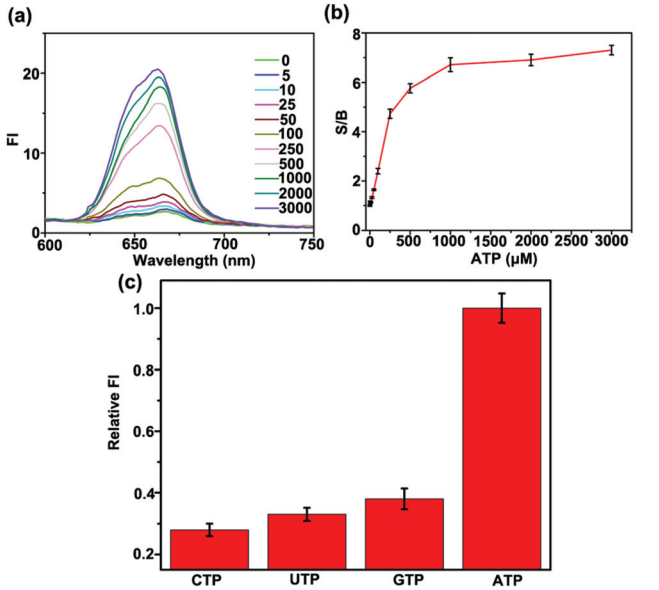

Fig. 3 (a) Fluorescence spectra of the nanoprobe (200 nM Ce6 equiv.) in the presence of different concentrations of ATP (μM). (b) Signal to background ratio (S/B) of nanoprobe fluorescence (200 nM Ce6 equiv.) as a function of ATP concentration. (c) Relative FI of the nanoprobe (200 nM Ce6 equiv.) in response to CTP, UTP, GTP, and ATP (1 mM) using ATP as the reference. λ_{ex} = 404 nm.

After replacing ATP with its analogues such as CTP, UTP and GTP at the same concentration to perform the fluorescence response experiment, only a little fluorescence recovery could be observed (Fig. 3c), indicating the acceptable selectivity of the designed nanoprobe toward ATP. This demonstrated the feasibility of the nanoprobe for ATP detection in a complex biological environment.

Evaluation of $^1O_2$ generation upon irradiation

To evaluate ATP-triggered $^1O_2$ generation, DPBF, a commonly used singlet oxygen indicator, was employed. DPBF can react irreversibly with oxygen species such as singlet oxygen to yield an endoperoxide product, leading to a reduction of the optical

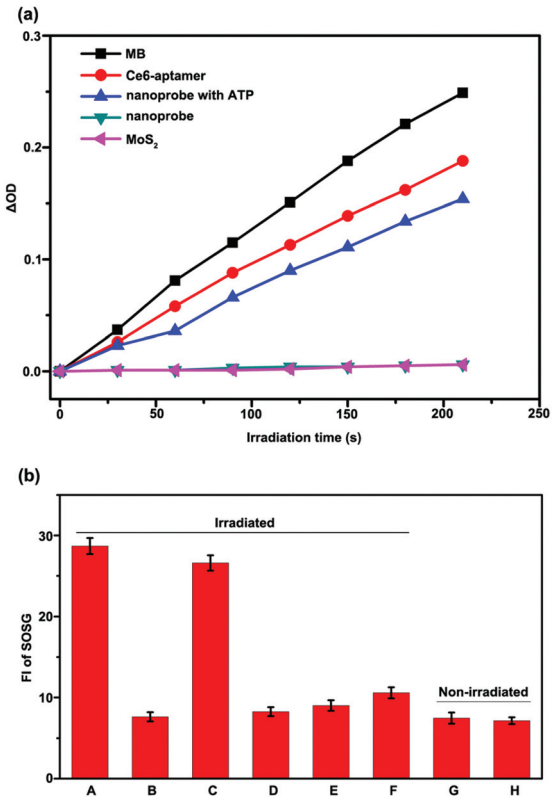

Fig. 4 (a) Plots of changes in the absorbance (ΔOD) of DPBF in marked solutions at 410 nm *vs.* irradiation time (λ = 660 nm) against MB as the standard in DMF. (b) $^1O_2$ generation in different solutions determined by the fluorescence intensity (FI) of SOSG at 525 nm: Ce6-aptamer (A), nanoprobe (0.5 μM Ce6 equiv.) without (B) and with 1 mM ATP (C), CTP (D), UTP (E), GTP (F) addition under 660 nm irradiation with a power of 0.22 W cm^{-2} and an irradiation dose of 66 J cm^{-2}, and the Ce6-aptamer (G), the nanoprobe with ATP (H) without irradiation.

density at 410 nm.[43] The nanoprobe solution showed an almost unchanged absorbance of DPBF at 410 nm with increasing irradiation time as MoS_2 did (Fig. 4a), suggesting the inhibition of $^1O_2$ generation by MoS_2. Upon addition of ATP, the change in absorbance (ΔOD) became gradually greater, indicating that the Ce6 was activated due to the binding of the aptamer with ATP and the release of the Ce6-aptamer from MoS_2. The restoration extent of $^1O_2$ generation was a little lower than that for the Ce6-aptamer, which might be owing to the incomplete departure of the Ce6-aptamer from the nanoplate. Using MB as the standard, the Φ for each sample was obtained (Table 1). A significant difference could be observed between the samples with and without ATP addition. Therefore, it was reasonable to conclude that the proposed nanoprobe possessed the ability of ATP-triggered $^1O_2$ generation.

To further demonstrate the ATP-triggered $^1O_2$ generation, an agent highly selective for $^1O_2$, SOSG,[35] was also employed for chemical detection of $^1O_2$, which exhibits an enhancement in the FI at 525 nm after reaction with $^1O_2$. In Fig. 4b, the FI of SOSG fluorescence of the nanoprobe upon irradiation showed

Table 1 Singlet oxygen quantum yields (Φ) for the Ce6-aptamer, the nanoprobe with ATP, the nanoprobe and MoS_2 in HEPES buffer

Samples	Singlet oxygen quantum yields (Φ)
Ce6-aptamer	0.389
Nanoprobe with ATP	0.324
Nanoprobe	0.041
MoS_2	0.032

a non-distinctive change compared with that of the nanoprobe without irradiation. However, in the presence of 1 mM ATP, the SOSG fluorescence of the nanoprobe upon exposure to light was greatly enhanced, which almost reached the level of the free Ce6-aptamer. This illustrated that the $^1O_2$ generation can be efficiently switched off by MoS_2 and switched on by the addition of ATP. Further study was carried out to study the interference of other nucleotides in the process of triggering of $^1O_2$ generation. Upon addition of CTP, UTP and GTP separately to a nanoprobe solution, only a small increase of the FI could be observed (Fig. 4b), which was similar to that of only the nanoprobe. These results stated well that the $^1O_2$ generation of the nanoprobe was specifically controlled by ATP.

In situ imaging of ATP in living cells

Prior to ATP imaging in the living cells, the cytotoxicity of MoS_2 nanoplates was compared with GO by the standard MTT assay (Fig. S3†). The HeLa cells incubated with MoS_2 nanoplates displayed higher cell viability compared with that of GO-incubated cells. This result is in good agreement with a previous report.[29] After the HeLa cells were incubated with the nanoprobe, MoS_2/Ce6-R and the Ce6-aptamer, respectively, a significant fluorescence signal was clearly observed from HeLa cells incubated with the nanoprobe (Fig. 5a), while little fluorescence was obtained from HeLa cells incubated with MoS_2/

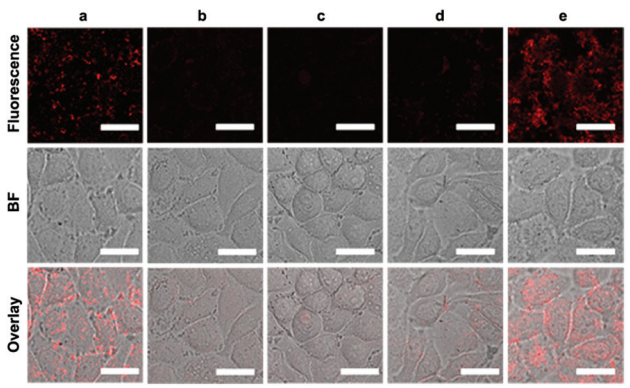

Fig. 5 Confocal microscopy fluorescence (top), bright field (BF) (middle), and the overlay (bottom) images of HeLa cells after incubation with the nanoprobe (2.0 μM Ce6 equiv.) (a), MoS_2/Ce6-R (2.0 μM Ce6 equiv.) (b), the Ce6-aptamer (2.0 μM Ce6 equiv.) (c), and 10 μg mL^{-1} oligomycin (d) or 5 mM Ca^{2+} (e) followed by incubation with the nanoprobe (2.0 μM Ce6 equiv.). Scale bar: 25 μm.

Ce6-R (Fig. 5b), suggesting that the nanoprobe had good specificity toward ATP in living cells. However, when using the Ce6-aptamer without MoS_2 to replace the nanoprobe, almost no fluorescence was observed (Fig. 5c), which might be owing to the poor delivery of the Ce6-aptamer into the cells without the assistance of MoS_2. In addition, to further prove that the fluorescence signal was triggered by the endogenous ATP, we conducted an ATP depletion experiment with oligomycin, a common inhibitor of ATP,[32,44] as well as an ATP increase experiment with Ca^{2+}, a well-known inducer of ATP.[32,45] Upon ATP depletion by oligomycin, a significant reduction of fluorescence signal was observed in the cells (Fig. 5d), while the ATP increase experiment showed a great increase after Ca^{2+} treatment (Fig. 5e). All these results indicated that the nanoprobe could effectively achieve *in situ* monitoring of ATP in living cells. Considering that ATP is much more abundant within the cells, the ATP-specific response of the proposed nanoprobe could be used as the switch for PDT implementation, thus enabling on-demand PDT. This would contribute to the reduction of the PDT dose and thus relieve pain during treatment. The incubation time of HeLa cells with the nanoprobe was optimized to be 6 h (Fig. S4†).

PDT with the nanoprobe

Low dark and strong light cytotoxicity to cells is necessary for therapeutic agents to achieve PDT. Thus the PDT effect of the proposed nanoprobe was evaluated by propidium iodide (PI)[46] fluorescence imaging of cells with different treatments. As shown in Fig. 6, cells untreated or treated with either a laser or nanoprobe only displayed negligible fluorescence of PI, while cells treated by the combination of the nanoprobe and the laser exhibited a significant PI fluorescence signal, which suggested obvious cell death. These results were also verified by MTT assays, as shown in Fig. S5.† These results demonstrated the strong PDT capability of the nanoprobe against the cancer cells. The light and dark cytotoxicity of the nanoprobe was also studied by MTT (Fig. S6a†) and flow cytometric assays (Fig. S6b†) with and without 660 nm laser exposure. The MTT assay indicated that the nanoprobe had little dark toxicity to cells with cell viability of more than 80% in the concentration range of 0–2.5 μM (Ce6 equiv.). However, the cell viability highly decreased with the increase of nanoprobe dose under 66 J cm^{-2} laser irradiation. When the concentration of the nanoprobe reached 2.5 μM (Ce6 equiv.), the growth inhibition (%) of cells was 77%, which was very close to that of 80% for the graphene oxide-based nanoprobe.[42] Flow cytometric analysis using the dual fluorescence of Annexin V-FITC/PI[37] confirmed the above results. As displayed in Fig. S6b,† when the cells were treated with the nanoprobe combined with the laser exposure, the cell mortality rate was high and increased with the enhanced light dose. The mortality rate reached up to 82.38% with a light dose of 66 J cm^{-2}, suggesting the promising PDT efficacy of the proposed nanoprobe. To study the role of ATP during the PDT process, oligomycin was introduced before the irradiation (Fig. 6). In the presence of 10 μg mL^{-1} oligomycin, the fluorescence of PI was hardly present, consistent with that shown in Fig. S5.† These results indicated that the PDT was indeed mediated by ATP.

The function of $^1O_2$ in the PDT process was also investigated using vitamin C as the ROS scavenger.[37] In the presence of 5 mM vitamin C, the cells displayed little PI signal similar to that for the untreated cells (Fig. 6), and the cell viability was high (Fig. S5†), suggesting that vitamin C effectively inhibited cell death. Therefore, it was reasonable to conclude that $^1O_2$ is responsible for the nanoprobe-mediated cell death.

To exclude the contribution of the photothermal effect of the nanoprobe to cell death, the temperature changes of MoS_2 nanoplate solution and water upon irradiation with a 660 nm laser intensity of 0.5 W cm^{-2} for different periods were monitored (Fig. S5c†). Different from the water sample, the MoS_2 nanoplate solution did not display an obvious temperature increase. This suggested that MoS_2 nanoplates showed little photothermal effect under 660 nm laser irradiation, thereby ruling out the possibility of photothermal therapy.

Mechanism of cell death during nanoprobe-mediated PDT

It is reported that different targets of PDT, such as endo/lysosomes, mitochondria, the nucleus, and the endoplasmic reticulum can induce cell death with different mechanisms.[37,47] For example, mitochondria, the main target of PDT, induce cell death with such a pathway consisting of mitochondrial depolarization, swelling, release of cytochrome c and apoptosis-inducing factor.[37,48] Lysosomes, another important target of PDT, lead to cell death through a lysosomal pathway such as the disruption of lysosomal membranes and release of lysosomal enzymes, for example cathepsins, into the cytosol.[37,49,50] Hence, it is really meaningful to localize the nanoprobe to reveal the mechanism of the nanoprobe-mediated PDT. Here a nucleus tracker, Hoechst 33342, and a lysosomal tracker, LysoTracker Green DND-26, were adopted for the colocalization assay.[47] As shown in Fig. 7, the fluorescence signal of Ce6 was well overlaid with the LysoTracker Green fluorescence, indicating that the nanoprobe was mainly distributed in the lysosomes and switched on by lysosomal ATP. This result also suggested that the nanoprobe might be triggered by these lysosomal ATP to mediate PDT. The produced $^1O_2$ induced the

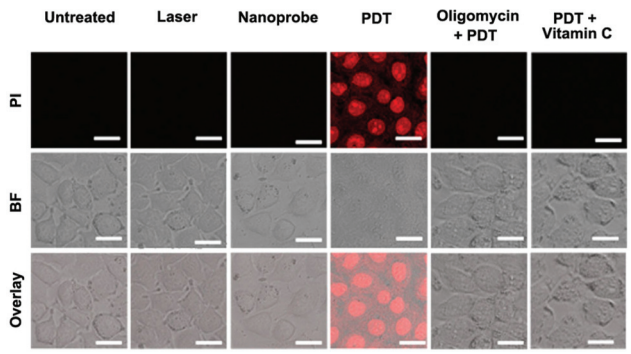

Fig. 6 Confocal fluorescence images of HeLa cells with different treatments using PI staining. Scale bars: 25 μm.

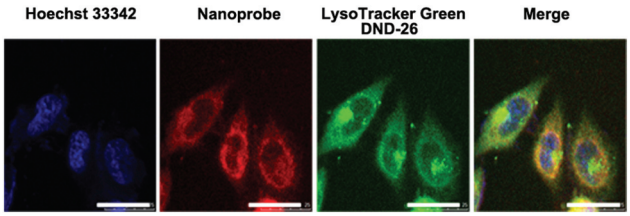

Fig. 7 Co-staining of nanoprobe-loaded HeLa cells with LysoTracker Green DND-26 and Hoechst 33342. Scale bars: 25 μm.

lysosomal membrane permeability and the release of lysosomal enzymes into the cytosol, leading to the execution of the apoptotic program.[50] Hence, the nanoprobe-mediated PDT induced cell death through the lysosomal pathway.[37]

Conclusions

We have synthesized a smart MoS_2 nanoplate-based nanoprobe to achieve fluorescence imaging of intracellular ATP and ATP-controllable PDT. The MoS_2 nanoplates possess good biocompatibility and high loading efficiency of the Ce6-aptamer. The Ce6-aptamer loaded MoS_2 can specifically respond to ATP by recovery of Ce6 fluorescence and thus achieve *in situ* "off–on" monitoring of ATP in living cells. The nanoprobe has low dark toxicity and can be activated by ATP to produce $^1O_2$ under laser irradiation in the lysosomes for inducing cell death by the lysosomal pathway, leading to on-demand PDT. Overall, our study presents an intelligent multifunctional theranostic platform for cellular imaging and controllable cancer therapy with excellent efficacy.

Acknowledgements

We gratefully acknowledge the National Natural Science Foundation of China (21135002, 21322506, 91213301, 91413118) and the National Basic Research Program (2014CB744501).

Notes and references

1 J. N. Coleman, M. Lotya, A. O'Neill, S. D. Bergin, P. J. King, U. Khan, K. Young, A. Gaucher, S. De, R. J. Smith, I. V. Shvets, S. K. Arora, G. Stanton, H.-Y. Kim, K. Lee, G. T. Kim, G. S. Duesberg, T. Hallam, J. J. Boland, J. J. Wang, J. F. Donegan, J. C. Grunlan, G. Moriarty, A. Shmeliov, R. J. Nicholls, J. M. Perkins, E. M. Grieveson, K. Theuwissen, D. W. McComb, P. D. Nellist and V. Nicolosi, *Science*, 2011, **331**, 568–571.
2 K. G. Zhou, N. N. Mao, H. X. Wang, Y. Peng and H. L. Zhang, *Angew. Chem., Int. Ed.*, 2011, **50**, 10839–10842.
3 H. Li, J. Wu, Z. Y. Yin and H. Zhang, *Acc. Chem. Res.*, 2014, **47**, 1067–1075.
4 Z. Y. Zeng, Z. Y. Yin, X. Huang, H. Li, Q. Y. He, G. Lu, F. Boey and H. Zhang, *Angew. Chem., Int. Ed.*, 2011, **50**, 11093–11097.
5 L. Cheng, J. J. Liu, X. Gu, H. Gong, X. Z. Shi, T. Liu, C. Wang, X. Y. Wang, G. Liu, H. Y. Xing, W. B. Bu, B. Q. Sun and Z. Liu, *Adv. Mater.*, 2014, **26**, 1886–1893.
6 M. Chhowalla, H. S. Shin, G. Eda, L. J. Li, K. P. Loh and H. Zhang, *Nat. Chem.*, 2013, **5**, 263–275.
7 C. L. Tan, Z. D. Liu, W. Huang and H. Zhang, *Chem. Soc. Rev.*, 2015, **44**, 2615–2628.
8 C. L. Tan and H. Zhang, *Chem. Soc. Rev.*, 2015, **44**, 2713–2731.
9 X. Huang, C. L. Tan, Z. Y. Yin and H. Zhang, *Adv. Mater.*, 2014, **26**, 2185–2204.
10 X. Huang, Z. Y. Zeng and H. Zhang, *Chem. Soc. Rev.*, 2013, **42**, 1934–1946.
11 G. Z. Sun, X. Zhang, R. Z. Lin, J. Yang, H. Zhang and P. Chen, *Angew. Chem., Int. Ed.*, 2015, **54**, 4651–4656.
12 G. Z. Sun, J. Q. Liu, X. Zhang, X. W. Wang, H. Li, Y. Yu, W. Huang, H. Zhang and P. Chen, *Angew. Chem., Int. Ed.*, 2014, **53**, 12576–12580.
13 B. Radisavljevic, A. Radenovic, J. Brivio, V. Giacometti and A. Kis, *Nat. Nanotechnol.*, 2011, **6**, 147–150.
14 Z. Y. Yin, Z. Y. Zeng, J. Q. Liu, Q. Y. He, P. Chen and H. Zhang, *Small*, 2013, **9**, 727–731.
15 Z. Y. Yin, H. Li, H. Li, L. Jiang, Y. M. Shi, Y. H. Sun, G. Lu, Q. Zhang, X. D. Chen and H. Zhang, *ACS Nano*, 2012, **6**, 74–80.
16 M. A. Lukowski, A. S. Daniel, F. Meng, A. Forticaux, L. S. Li and S. Jin, *J. Am. Chem. Soc.*, 2013, **135**, 10274–10277.
17 T. Y. Wang, H. C. Zhu, J. Q. Zhuo, Z. W. Zhu, P. Papakonstantinou, G. Lubarsky, J. Lin and M. X. Li, *Anal. Chem.*, 2013, **85**, 10289–10295.
18 X. Huang, Z. Y. Zeng, S. Y. Bao, M. F. Wang, X. Y. Qi, Z. X. Fan and H. Zhang, *Nat. Commun.*, 2013, **4**, 1444.
19 J. Z. Chen, X. J. Wu, L. S. Yin, B. Li, X. Hong, Z. X. Fan, B. Chen, C. Xue and H. Zhang, *Angew. Chem., Int. Ed.*, 2015, **54**, 1210–1214.
20 C. F. Zhu, Z. Y. Zeng, H. Li, F. Li, C. H. Fan and H. Zhang, *J. Am. Chem. Soc.*, 2013, **135**, 5998–6001.
21 Y. Zhang, B. Zheng, C. F. Zhu, X. Zhang, C. L. Tan, H. Li, B. Chen, J. Yang, J. Z. Chen, Y. Huang, L. H. Wang and H. Zhang, *Adv. Mater.*, 2015, **27**, 935–939.
22 Y. Chen, C. L. Tan, H. Zhang and L. Z. Wang, *Chem. Soc. Rev.*, 2015, **44**, 2681–2701.
23 W. Y. Yin, L. Yan, J. Yu, G. Tian, L. J. Zhou, X. P. Zheng, X. Zhang, Y. Yong, J. Li, Z. J. Gu and Y. L. Zhao, *ACS Nano*, 2014, **8**, 6922–6933.
24 S. S. Chou, B. Kaehr, J. Kim, B. M. Foley, M. De, P. E. Hopkins, J. X. Huang, C. J. Brinker and V. P. Dravid, *Angew. Chem., Int. Ed.*, 2013, **52**, 4160–4164.
25 T. Liu, C. Wang, W. Cui, H. Gong, C. Liang, X. Z. Shi, Z. W. Li, B. Q. Sun and Z. Liu, *Nanoscale*, 2014, **6**, 11219–11225.
26 J. Li, F. Jiang, B. Yang, X. R. Song, Y. Liu, H. H. Yang, D. R. Cao, W. R. Shi and G. N. Chen, *Sci. Rep.*, 2013, **3**, 1998.

27 T. Liu, S. X. Shi, C. Liang, S. D. Shen, L. Cheng, C. Wang, X. J. Song, S. Goel, T. E. Barnhart, W. B. Cai and Z. Liu, *ACS Nano*, 2015, **9**, 950–960.
28 T. Liu, C. Wang, X. Gu, H. Gong, L. Cheng, X. Z. Shi, L. Z. Feng, B. Q. Sun and Z. Liu, *Adv. Mater.*, 2014, **26**, 3433–3440.
29 W. Z. Teo, E. L. K. Chng, Z. Sofer and M. Pumera, *Chem. – Eur. J.*, 2014, **20**, 9627–9632.
30 P. Huang, Z. M. Li, J. Lin, D. P. Yang, G. Gao, C. Xu, L. Bao, C. L. Zhang, K. Wang, H. Song, H. Y. Hu and D. X. Cui, *Biomaterials*, 2011, **32**, 3447–3458.
31 H. Imamura, K. P. H. Nhat, H. Togawa, K. Saito, R. Iino, Y. Kato–Yamada, T. Nagai and H. Noji, *Proc. Natl. Acad. Sci. U. S. A.*, 2009, **106**, 15651–15656.
32 M. Yi, S. Yang, Z. Y. Peng, C. H. Liu, J. S. Li, W. W. Zhong, R. H. Yang and W. H. Tan, *Anal. Chem.*, 2014, **86**, 3548–3554.
33 R. Mo, T. Y. Jiang and Z. Gu, *Angew. Chem., Int. Ed.*, 2014, **53**, 5815–5820.
34 M. Naito, T. Ishii, A. Matsumoto, K. Miyata, Y. Miyahara and K. Kataoka, *Angew. Chem., Int. Ed.*, 2012, **51**, 10751–10755.
35 Z. Zhu, Z. W. Tang, J. A. Phillips, R. H. Yang, H. Wang and W. H. Tan, *J. Am. Chem. Soc.*, 2008, **130**, 10856–10857.
36 Q. Cao, K. X. Zhao, X. Z. Zhong, Y. J. Zou, H. C. Yu, P. Huang, T. L. Xu and X. P. Dong, *J. Biol. Chem.*, 2014, **289**, 23189–23199.
37 J. W. Tian, L. Ding, H. J. Xu, Z. Shen, H. X. Ju, L. Jia, L. Bao and J. S. Yu, *J. Am. Chem. Soc.*, 2013, **135**, 18850–18858.
38 X. D. Zhang, X. Xie, H. Wang, J. J. Zhang, B. C. Pan and Y. Xie, *J. Am. Chem. Soc.*, 2013, **135**, 18–21.
39 D. Gopalakrishnan, D. Damien and M. M. Shaijumon, *ACS Nano*, 2014, **8**, 5297–5303.
40 S. S. Chou, M. De, J. Kim, S. Byun, C. Dykstra, J. Yu, J. X. Huang and V. P. Dravid, *J. Am. Chem. Soc.*, 2013, **135**, 4584–4587.
41 B. Tian, C. Wang, S. Zhang, L. Z. Feng and Z. Liu, *ACS Nano*, 2011, **5**, 7000–7009.
42 J. W. Tian, L. Ding, Q. B. Wang, Y. P. Hu, L. Jia, J. S. Yu and H. X. Ju, *Anal. Chem.*, 2015, **87**, 3841–3848.
43 N. Adarsh, R. R. Avirah and D. Ramaiah, *Org. Lett.*, 2010, **12**, 5720–5723.
44 Z. C. Xu, N. J. Singh, J. Lim, J. Pan, H. N. Kim, S. Park, K. S. Kim and J. Yoon, *J. Am. Chem. Soc.*, 2009, **131**, 15528–15533.
45 H. J. Kennedy, A. E. Pouli, E. K. Ainscow, L. S. Jouaville, R. Rizzuto and G. A. Rutter, *J. Biol. Chem.*, 1999, **274**, 13281–13291.
46 J. Wang, G. Z. Zhu, M. X. You, E. Song, M. I. Shukoor, K. J. Zhang, M. B. Altman, Y. Chen, Z. Zhu, C. Z. Huang and W. H. Tan, *ACS Nano*, 2012, **6**, 5070–5077.
47 H. B. Chen, L. Xiao, Y. Anraku, P. Mi, X. Y. Liu, H. Cabral, A. Inoue, T. Nomoto, A. Kishimura, N. Nishiyama and K. Kataota, *J. Am. Chem. Soc.*, 2014, **136**, 157–163.
48 M. Lam, N. L. Oleinick and A. L. Nieminen, *J. Biol. Chem.*, 2001, **276**, 47379–47386.
49 J. W. Tian, L. Ding, H. X. Ju, Y. C. Yang, X. L. Li, Z. Shen, Z. Zhu, J. S. Yu and C. Y. J. Yang, *Angew. Chem., Int. Ed.*, 2014, **53**, 9544–9549.
50 M. E. Guicciardi, M. Leist and G. J. Gores, *Oncogene*, 2004, **23**, 2881–2890.